Determination of the bulk band structure of Ag in Ag/Cu(111) quantum-well systems

M. A. Mueller, T. Miller, and T.-C. Chiang
Department of Physics, University of Illinois at Urbana-Champaign, 1110 West Green Street, Urbana, Illinois 61801 and Materials Research Laboratory, University of Illinois at Urbana-Champaign, 104 South Goodwin Avenue, Urbana, Illinois 61801
(Received 17 August 1989)

Ag is grown epitaxially on Cu(111) to form quantum wells. The resulting quantum-well states and resonances, observed with angle-resolved photoemission, exhibit shifts in energy for varying emission directions and for changing Ag-film thicknesses. The results are utilized in a determination of the Ag bulk *sp*-band dispersion relation near the L point in the Brillouin zone. Effective masses and the Fermi surface near the L point are deduced. The Fermi surface agrees well with that obtained earlier from de Haas–van Alphen measurements.

I. INTRODUCTION

One very important application of angle-resolved photoemission is the three-dimensional mapping of bulk valence bands in crystals. Until recently, bands could be mapped only by assuming a reasonable form for a final-state band.[1] Although $k_\perp$ is practically conserved during the photoexcitation process, $k_\perp$ information is partially lost as the photoelectron escapes into vacuum. By observing a thin film instead of a bulk crystal, it is possible to determine valence-band dispersion without making any assumptions about the final band since $k_\perp$ for the initial state can be found from the requirement of quantization along the direction of the film thickness. This has been pointed out in an earlier theoretical treatment.[2] A similar determination can also be made with tunneling measurements,[3] although there remains a question concerning the selectivity of $k_\parallel$ since the electron does not necessarily tunnel in a direction normal to the film. Such tunneling measurements also generally require cryogenic temperatures. The first photoemission observation of quantized states in a film was, to our best knowledge, reported for Ag/Si(111).[4] Later, similar observations have been reported for Ag/Si(111),[5] Ag/Ge(111),[6] Na/Cu(111),[7] Ba/Cu(111),[7] Ag/Au(111),[8] Cs/Cu(111),[9] Ag/Cu(111),[10] etc. These studies have demonstrated the commonness of the quantum-well effects and the usefulness of the application of normal emission to quantum wells in mapping bulk $E(k_\perp)$ of the overlayer material. This paper is a followup of our earlier Rapid Communication of the Ag/Cu(111) system to include details,[10] and the results will be compared with those from Ag/Au(111) obtained in a parallel study.[8] Most importantly, the work has been extended to off-normal-emission geometries to obtain a detailed picture for the Ag *sp* band near the Fermi level. The shape of the Fermi surface in **k** space near the L critical point is deduced, which agrees well with that deduced from earlier de Haas–van Alphen measurements.

The Ag/Cu(111) quantum well is nearly ideal for exploring the behavior of off-normal emission. The quantum-well states and resonances have been observed over the widest range of binding energies in a normal-emission geometry for any overlayer-substrate combination so far observed. This system probably also shows the best film structure, allowing a fairly wide range of polar emission angles to be employed.

II. EXPERIMENTAL DETAILS

The experiments were performed at the Synchrotron Radiation Center of the University of Wisconsin–Madison at Stoughton, Wisconsin. Two different monochromators, a 6-m toroidal grating monochromator and a normal-incidence monochromator, were utilized during several separate runs. The photoemitted electrons were analyzed with a hemispherical analyzer which exhibits a 3° full acceptance angle. The Cu(111) substrate was oriented to within 0.5° by x-ray diffraction, and was prepared by mechanical polishing followed by electropolishing to remove the mechanically damaged layer. It was treated in the vacuum chamber by cycles of Ar-ion sputtering and annealing until a sharp (1×1) electron diffraction pattern was observed. The surface quality was verified by the observation of a sharp surface state in the normal-emission spectra just below the Fermi level.[11] The alignment of the analyzer relative to the sample crystallographic axes was facilitated by electron diffraction inside the chamber and by optical methods using the visible part of the synchrotron beam to find the sample surface-normal direction. The angular alignment was better than 1°.

The Ag overlayers were prepared by evaporation from a tungsten crucible heated by a feedback-controlled electron beam. The overlayers were annealed briefly at 200 °C to enhance the film uniformity. Growth of Ag on Cu(111) under these conditions has been extensively studied before; the Ag grows in the (111) orientation with its own natural lattice constant. Even though the Ag and Cu lattices are not matched, the quality of the Ag film is excellent as ascertained by the results of previous Ag/Cu(111) experiments.[10,12] As with the Cu(111) sample, the overlayer surface quality is verified by observation of a sharp (1×1) electron diffraction pattern and

Ag(111) surface-state peak. The Ag film thickness was monitored with a water-cooled quartz thickness monitor, which was calibrated absolutely by a method similar to that reported in Ref. 12. The uncertainty for the absolute film thickness is about 10%. The photoemission measurements were performed with the sample at nearly room temperature.

III. RESULTS AND DISCUSSION

A. Normal-emission results for Ag/Cu(111)

A typical set of normal-emission spectra for various Ag film thicknesses on Cu(111), produced with $h\nu=10$ eV photons, is shown in Fig. 1. The film thickness is given here in terms of the Ag(111) monolayer (ML). The large peaks near the Fermi level E_F are Ag(111) surface-state peaks,[12] and the smaller peaks at higher binding energies represent quantum-well states or resonances within the Ag overlayer as reported previously.[10] For brevity, we will refer to both quantum-well states and resonances as quantum states. These states are seen evolving as a function of film thickness, becoming more crowded as the film grows thicker. At the largest film thickness shown here (43 ML), the first quantum state just below the surface state begins to fade away. At even larger thicknesses, more of the states begin to disappear; such behavior is consistent with limitations imposed by a finite resolution. As discussed previously,[2–10] the energy positions of the quantum-state peaks are given by

$$2k_\perp(E)d+\delta(E)=2n\pi\ , \tag{1}$$

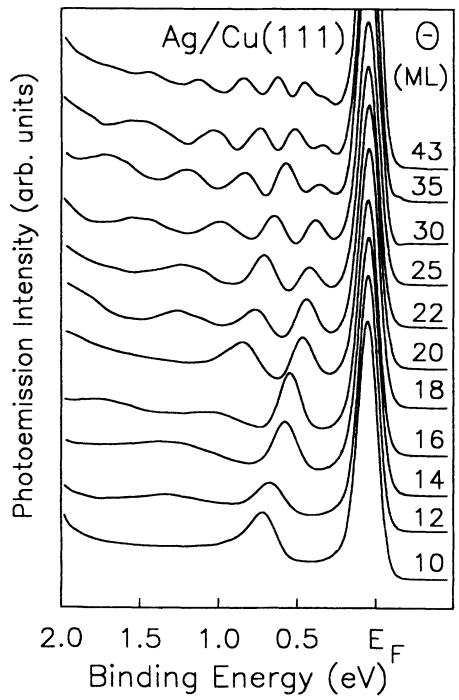

FIG. 1. Normal-emission spectra taken, with $h\nu=10$ eV photons, of various Ag coverages on Cu(111). The binding-energy scale is referred to the Fermi level E_F, and the coverage Θ is expressed in terms of Ag(111) monolayers (ML).

where d is the quantum-well thickness, $k_\perp$ is the component of the electron wave vector along the surface normal [111] direction, δ is the sum of the phase shifts at the Ag-Cu and Ag-vacuum boundaries, E is the electron energy, and n is a quantum number (integer). In this expression, we have ignored a possible small thickness dependence of $k_\perp$ and δ due to nonlocal effects. This should be an excellent approximation, since the metallic screening length is extremely short compared to the film thicknesses employed in this experiment. An electron located more than just $\sim\frac{1}{2}$ Å away from either boundary of the film is well shielded from the surface or interface potential, and its motion should be essentially the same as that in the bulk. Thus, $k_\perp(E)$ in Eq. (1) is just the bulk band dispersion of Ag along the surface-normal direction. Likewise, the phase shift at one boundary should not depend on the potential variation at the other boundary; the only relevant parameter is the electron energy. The quantum-well thickness d in Eq. (1) will be taken as the nominal film thickness here; the error for each boundary is at most on the order of the screening length ($\sim\frac{1}{2}$ Å), which is only 2–0.5 % of the film thicknesses used in this study (24–100 Å).

The neighboring quantum-state peaks in each spectrum shown in Fig. 1 correspond to successive values of the integer quantum number n. Such data can be processed to yield a dispersion relation of the Ag(111) sp band along the [111] direction.[9,10] Briefly, if quantum state n for Ag thickness d happens to have the same energy E as that of quantum state n' ($n'=n+1$, for example) for Ag thickness d', then the simultaneous solution of Eq. (1) for the two thicknesses yields

$$k_\perp=\pi(n'-n)/(d'-d)\ . \tag{2}$$

Since only the difference $n'-n$ appears in the result, the absolute value of n, which depends on the choice of origin, is not important. Similarly, since only the difference $d'-d$ appears in the result, the error introduced by ignoring a possible difference between the quantum-well thickness and the nominal film thickness is minimized. The 10% error in absolute film thickness leads to a corresponding 10% error in the $k_\perp$ value so determined. The resulting $E(k_\perp)$ data from Ag/Cu(111) are shown in Fig. 2 as solid squares, which correspond to the band dispersion of the Ag sp state; the origin of the abscissa is chosen to be at the L point in the bulk Brillouin zone. The results agree very well with the "best estimate" reported by Nelson *et al.* based on a photoemission study and theoretical calculations.[13] The solid curve shown in Fig. 2 is a fit to the Ag/Cu(111) data based on the usual two-band model.[10] The fitting function is

$$\varepsilon(k_\perp)=E-E_0+2\varepsilon(p)-U-[(2\varepsilon(p)-U)^2+4\varepsilon(p)(E-E_0)]^{1/2}\ , \tag{3}$$

where E (energy) is referred to the Fermi level, E_0 is the band-edge energy, $\varepsilon(x)\equiv\hbar^2x^2/2m_\perp^*$, $p\equiv\sqrt{3}\pi/a$ (a is the lattice constant), and $U=2.1$ eV is one-half of the sp gap energy. The fit gives $m_\perp^*/m=0.74$ and $E_0=-0.33$ eV.[10]

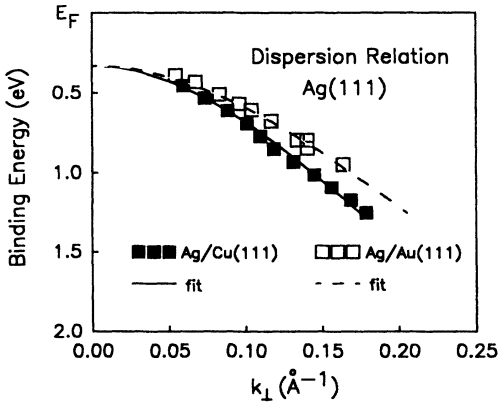

FIG. 2. The *sp*-band dispersion for Ag along the [111] direction. Solid squares are data points from Ag/Cu(111) systems, and open squares are from Ag/Au(111) systems. The solid curve is a least-squares fit of the Ag/Cu(111) points based on the two-band model. The dashed curve is obtained from the solid curve by multiplying the $k_\perp$ values by 1.17 to account for discrepancies in absolute thickness calibration (see text for details).

B. Comparison with results for Ag/Au(111)

Results for Ag/Au(111) have been similarly analyzed,[8,14] as shown in Fig. 2. The two data sets can be made consistent with a simple correction for the film-thickness calibration. The Ag/Cu and Ag/Au data were taken with independent calibrations. The dashed curve in Fig. 2 is obtained from the solid curve by multiplying $k_\perp$ by 1.17, which describes the Ag/Au(111) data well. This rescaling of $k_\perp$ corresponds to a 17% calibration difference.

Ag/Au(111) quantum states are observed clearly only at energies above the Au *sp*-band edge. This can be explained in terms of the degree of electron confinement.[8] Above the Au *sp*-band edge, electrons in the well are confined by energy conservation. Below the edge, partial reflection at the Ag-Au interface results in a much weaker partial confinement and the formation of quantum-well resonances. In contrast, sharp Ag/Cu(111) quantum peaks are observed both above and below the Cu *sp*-band edge with comparable intensities. The degree of confinement for Ag/Cu resonances appears to be greater. Perhaps the lattice mismatch between Ag and Cu causes a larger electron reflection coefficients. We have not found any calculations pertaining to such reflection coefficients.

C. Comparison with results from tunneling measurements

The Ag band dispersions have also been determined before by tunneling spectroscopy performed at liquid-helium temperature.[3] The temperature difference should not give rise to large changes in the band structure.[3,15] However, a comparison of the present Ag/Cu results with those deduced from earlier tunneling measurements shows a significant discrepancy. This could be due to an error in absolute film-thickness calibration, which was not specified in the earlier measurements. If we assume that the tunneling measurements underestimated the film thickness by about 35%, then the two sets of data agree. Also, the films studied in the tunneling measurements were prepared by evaporation onto an oxide surface at 90 K in medium vacuum and then annealed at room temperature. The resulting films were textured, and this structural difference might also contribute to the discrepancy.

Another point to be noted is that in the analysis of the earlier tunneling results, the phase shift δ in Eq. (1), was effectively neglected. There is not enough data in Ref. 3 for us to perform an analysis as done in this study. Since the phase shift is at most 2π, the error caused by ignoring δ in Eq. (1) is equivalent to an error of $\Delta n = 1$ in the assignment of the quantum number. An inspection of Fig. 20 in Ref. 3 shows that this is a relatively small error for the rather thick films employed in that study. Thus, a fairly accurate band dispersion can be obtained by analyzing the quantum-state peak positions for just one rather thick film, as done in Ref. 3.

D. Off-normal-emission results for Ag/Cu(111)

A very large number of spectra for Ag/Cu(111) were recorded for various overlayer thicknesses, photon energies, and emission angles. Figures 3 and 4 show two typical sets of spectra for a 30-ML Ag film on Cu(111) taken with photon energy $h\nu = 11$ eV; the emission directions are indicated and correspond to scanning along $\mathbf{k}_\parallel \| [1\bar{1}0]$ and $[11\bar{2}]$, respectively. Each set contains a spectrum for normal emission ($\theta = 0°$), and it is easy to follow the evolution of the peaks as the polar angle θ is varied in small

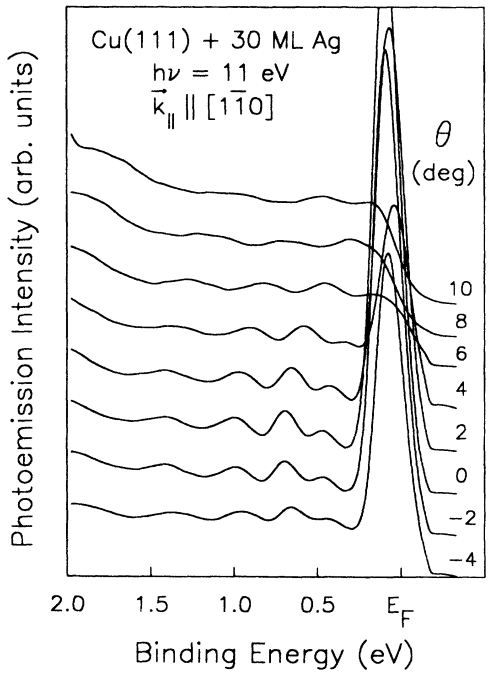

FIG. 3. Photoemission spectra for 30 ML of Ag on Cu(111) taken with $h\nu = 11$ eV. The polar emission angle θ and the direction of scan ($\mathbf{k}_\parallel \| [1\bar{1}0]$) are indicated.

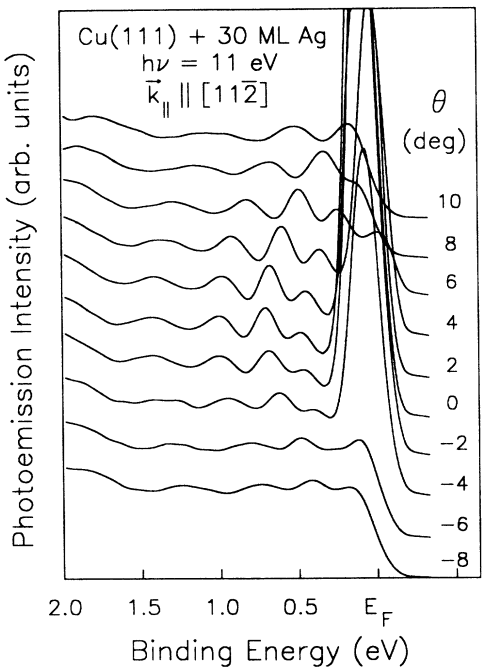

FIG. 4. Photoemission spectra for 30 ML of Ag on Cu(111) taken with $h\nu=11$ eV. The polar emission angle θ and the direction of scan ($\mathbf{k}_\parallel \| [11\bar{2}]$) are indicated.

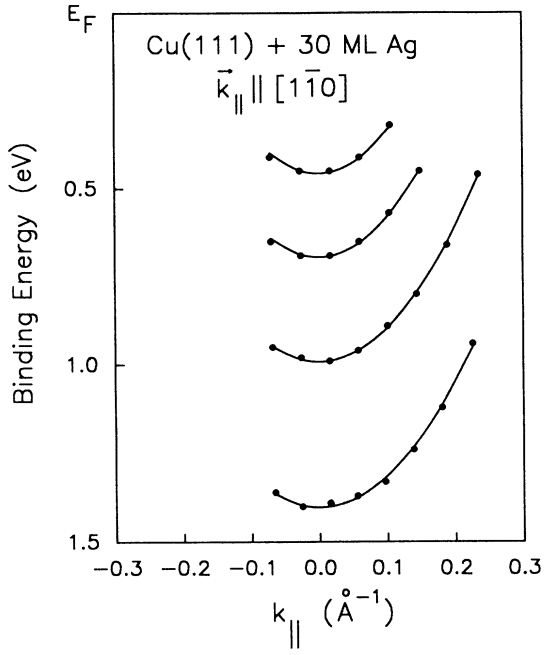

FIG. 5. Quantum-state $E(k_\parallel)$ data points derived from the spectra shown in Fig. 3.

steps. The surface-state and quantum-state peaks are all seen to move toward the Fermi level for increasing magnitude of θ, and some of these eventually cross the Fermi level and disappear. Also, the quantum-state peaks become less pronounced; this effect limits the useful range of scan for θ. The dispersive behavior of the surface-state peak is the same as that observed previously for the surface state on pure Ag(111).[16–18] The quantum-state peaks disperse as expected, based on the known bulk band structure of Ag.[18–20] Since $k_\perp$ is already fixed by the quantization rule given in Eq. (1), the scan for different angles corresponds to varying $\mathbf{k}_\parallel$. The measured dispersions of the quantum-state peaks directly yield the band dispersions at discrete $k_\perp$ intervals.

Figures 5 and 6 show the band dispersion relations for the various quantum-state peaks obtained from the data shown in Figs. 3 and 4, respectively. The $k_\parallel$ values are computed from the standard expression

$$k_\parallel=[2m(h\nu-E_B-\Phi)]^{1/2}\sin\theta/\hbar\ , \tag{4}$$

where m is the free-electron mass, E_B is the measured binding energy relative to the Fermi level, and $\Phi=4.49$ eV is the work function of Ag(111).[21] The curves in Figs. 5 and 6 are parabolic fits which are expected to be good approximations for small $k_\parallel$ values:

$$E_n(k_\parallel)=E_n(k_\parallel=0)+\hbar^2k_\parallel^2/2m_\parallel^*\ . \tag{5}$$

Here, E_n $(k_\parallel=0)$ and $m_\parallel^*$ (in-plane effective mass) are the fitting parameters. In the process of the analysis, a small angular correction $\Delta\theta<1°$ was applied for each set of data (corresponding to each independent run) to bring the minima of the parabolas to $k_\parallel=0$. The corrections compensate for small angular misalignments during the experiment. Figures 7 and 8 show similar band dispersion results obtained from a 24-ML Ag film on Cu(111) for scan directions $\mathbf{k}_\parallel \| [1\bar{1}0]$ and $[11\bar{2}]$, respectively. These results illustrate that the dispersive behaviors of the quantum-state peaks are qualitatively the same for different film thicknesses.

Figure 9 displays the values of the in-plane effective mass $m_\parallel^*$ obtained from the parabolic fits to the data for 9-, 18-, 24-, 27-, and 30-ML-thick films as a function of the binding energy at $k_\parallel=0$, namely, E_n $(k_\parallel=0)$. The

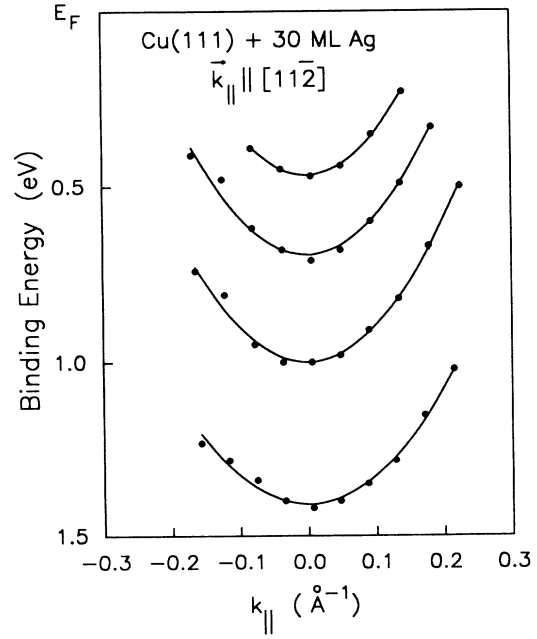

FIG. 6. Quantum-state $E(k_\parallel)$ data points derived from the spectra shown in Fig. 4.

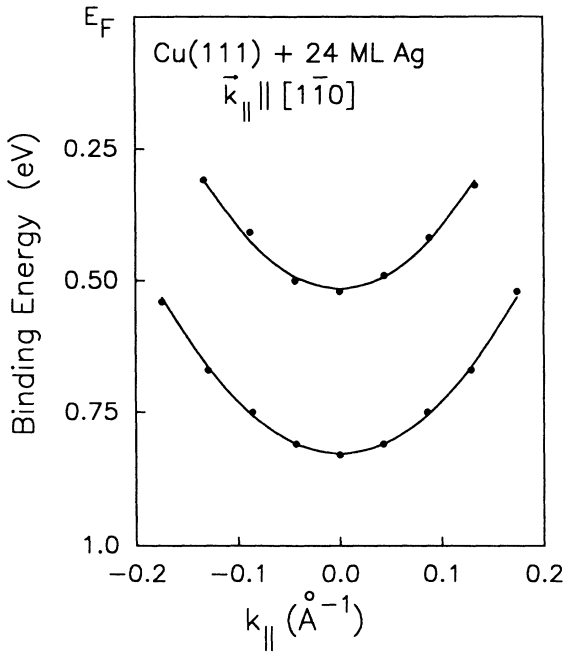

FIG. 7. Quantum-state $E(k_{\parallel})$ data points derived from off-normal-emission ($\mathbf{k}_{\parallel}\|[1\bar{1}0]$) spectra for a 24-ML Ag film on Cu(111).

triangles and inverted triangles correspond to scan directions $\mathbf{k}_{\parallel}\|[1\bar{1}0]$ and $[11\bar{2}]$, respectively; the two sets agree within the data scattering. This is expected since the (111) surface exhibits a threefold symmetry, and the in-plane effective mass at $\bar{\Gamma}$ should be isotropic. The straight line in Fig. 9 is a least-squares linear fit to all of the data:

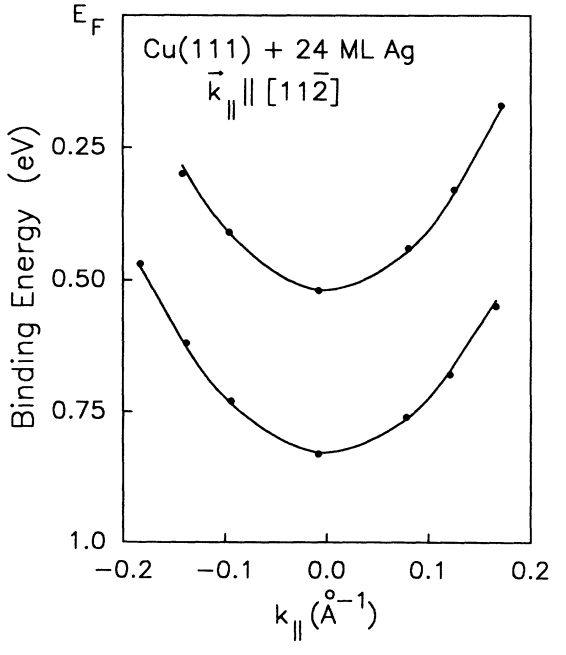

FIG. 8. Quantum-state $E(k_{\parallel})$ data points derived from off-normal-emission ($\mathbf{k}_{\parallel}\|[11\bar{2}]$) spectra for a 24-ML Ag film on Cu(111).

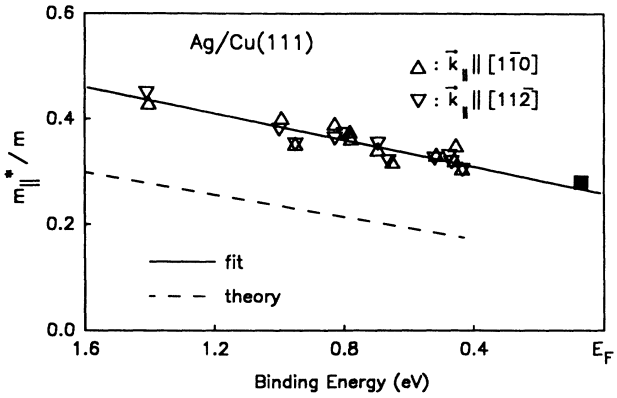

FIG. 9. In-plane effective mass $m_{\parallel}^{*}$ relative to the free-electron mass m as a function of the binding energy at $k_{\parallel}=0$. Triangles and inverted triangles represent data for $\mathbf{k}_{\parallel}\|[1\bar{1}0]$ and $[11\bar{2}]$ off-normal-emission data, respectively. The solid line is a linear fit to the data. A solid square marks the result for the Ag(111) surface state. Interpolated theoretical values are represented by the dashed line.

$$m_{\parallel}^{*}(E)/m = a + bE \ , \tag{6}$$

where $a=0.265$ and $b=0.120\ \mathrm{eV}^{-1}$. The results indicate that the effective masses obtained from films with different thicknesses are consistent, in agreement with the earlier statement that we are measuring the bulk band dispersions which should not depend on the quantum-well geometry. The $m_{\parallel}^{*}$ for the Ag(111) surface state from previous high-resolution work is also shown in Fig. 9 (the solid square).[16] It falls along the linear fit as expected, since the surface state can be reached by analytic continuation of the bulk states into the gap.

A linear interpolation of effective-mass values at the top and bottom of the *sp* band, derived from a theoretical Ag band-structure calculation,[18] is also displayed in Fig. 9 (dashed line). This line exhibits a slope comparable to that of the experimental fit.

E. Band dispersion and the Fermi surface of Ag

Equations (3), (5), and (6) together determine the Ag *sp*-band dispersion in three dimensions near the L point:

$$E(k_{\perp},k_{\parallel})=E(k_{\perp},0)+\hbar^{2}k_{\parallel}^{2}/\{2[a+bE(k_{\perp},0)]\} \ , \tag{7}$$

where a and b are the fitting parameters given above. The function $E(k_{\perp},0)$ is given by

$$E(k_{\perp},0)=E_{0}+\varepsilon(k_{\perp})+U-[4\varepsilon(k_{\perp})\varepsilon(p)+U^{2}]^{1/2} \ , \tag{8}$$

which is obtained by inverting Eq. (3) and keeping only the lower branch of the dispersion (since the region of interest is very close to the lower edge of the gap, the lower branch is the only one needed here).[17]

An interesting application of these results is a determination of the Fermi surface of bulk Ag. The Ag Fermi surface has been examined before based on the de Haas–van Alphen effect,[22–25] and is one of the standard examples used in textbooks to illustrate the concepts of Fermi surface and band structure.[26] Here, knowing the

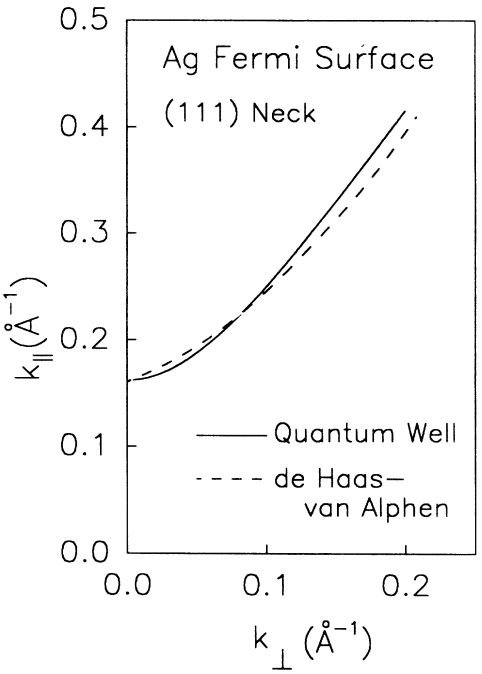

FIG. 10. The Ag Fermi surface (solid curve) determined from the quantum-well results. The dashed curve represents results determined from de Haas–van Alphen measurements.

function $E(k_{\perp},k_{\parallel})$, we determine the Fermi surface in terms of $k_{\perp}$ and $k_{\parallel}$ simply by setting $E(k_{\perp},k_{\parallel})=0$. Conceptually, the off-normal parabolic dispersion of a given quantum state (fixed $k_{\perp}$) toward, and intersecting with, the Fermi level as observed in Figs. 5–8, corresponds to the Brillouin-zone picture of the intersection of the Ag Fermi-surface neck with a plane of constant $k_{\perp}$, which is parallel to the hexagonal (111) Brillouin-zone face. The results of a numerical computation for the Fermi surface are shown graphically in Fig. 10 (solid curve). The de Haas–van Alphen results from Ref. 23 are also shown for comparison (dashed curve). The agreement is excellent considering the experimental uncertainties.[22–25] The radius of the (111) "neck" of the Fermi surface is 0.162 Å^{-1} from the present data, in excellent agreement with the de Haas–van Alphen results.

F. Lateral coherence length

Ag/Cu(111) exhibits quantum-state peaks which become smaller with increasing polar emission angles. This is evident in Figs. 3 and 4. The simplest explanation for the intensity decrease is that the well has a finite lateral coherence length. The quantum-well effect depends on coherence of the interfering wave functions arising from multiple bounces between the two film boundaries. An analogy is the Fabry-Perot interferometer; the contrast is reduced for off-normal-incidence direction because the light beam shifts sideways for each bounce at the mirrors, and the effective number of beams involved in the multibeam interference is reduced. Earlier work has shown that an effective scattering length of 20–30 Å accounts for the broadening of the Cu(111) surface state at room temperature.[27] Although it is difficult to analyze the data (see Figs. 3 and 4) to yield quantitative intensity and linewidth information, it appears that a lateral coherence length of 20–30 Å is consistent with the observed intensity decrease at nonzero emission angles.

IV. SUMMARY AND CONCLUSIONS

This work has shown that band dispersion relations can be obtained by measuring the energies of the quantum states in films as functions of the film thickness and the emission direction. The component of the wave vector perpendicular to the film, $k_{\perp}$, is determined by quantization due to the finite thickness of the film. The final band is not involved in this determination, and therefore this method is inherently more accurate than the usual methods of photoemission band mapping involving bulk single crystals. Off-normal scans allow the in-plane component of the wave vector, $\mathbf{k}_{\parallel}$, to be varied. From such measurements for Ag films grown on Cu(111), the three-dimensional band dispersion for the Ag *sp* band is obtained near the *L* critical point. The Fermi surface deduced from this analysis is in excellent agreement with that deduced from a de Haas–van Alphen study. The angular range of off-normal scans seems to be limited by lateral coherence lengths.

ACKNOWLEDGMENTS

This material is based on work supported by the National Science Foundation under Contract No. DMR-86-14234. Some of the personnel and equipment were also supported by grants from the National Science Foundation (Grant No. DMR-83-52083) and the E. I. du Pont de Nemours and Company (Wilmington, DE). The Synchrotron Radiation Center of the University of Wisconsin–Madison is supported by the National Science Foundation under Contract No. DMR-80-20164. We acknowledge use of the central facilities of the Materials Research Laboratory of the University of Illinois, which is supported by the U.S. Department of Energy (Division of Material Sciences of the Office of Basic Energy Sciences) under Contract No. DE-AC02-76ER01198, and by the National Science Foundation under Contract No. DMR-86-12860.

[1]See, for example, Y. Petroff, and P. Thiry, Appl. Opt. **19**, 3957 (1980); F. J. Himpsel, *ibid.* **19**, 3964 (1980).
[2]P. D. Loly and J. B. Pendry, J. Phys. C **16**, 423 (1983).
[3]R. C. Jaklevic and J. Lambe, Phys. Rev. B **12**, 4146 (1975).
[4]A. L. Wachs, A. P. Shapiro, T. C. Hsieh, and T.-C. Chiang, Phys. Rev. B **33**, 1460 (1986).
[5]T.-C. Chiang, in *Metallic Multilayers and Epitaxy,* edited by M. Hong, S. Wolf, and D. C. Gubser (The Metallurgical Society, AIME, Warrendale, PA, 1988), pp. 167–184.
[6]A. L. Wachs, T. Miller, A. P. Shapiro, and T.-C. Chiang, in *In-*

itial Stages of Epitaxial Growth, Vol. 94 of *Materials Research Society Symposium Proceedings,* edited by R. Hull, J. M. Gibson, and D. A. Smith (MRS, Pittsburgh, 1987), p. 225.

[7]S. Å. Lindgren and L Walldén, Phys. Rev. Lett. **59**, 3003 (1987).

[8]T. Miller, A. Samsavar, G. E. Franklin, and T.-C. Chiang, Phys. Rev. Lett. **61**, 1404 (1988).

[9]S. Å. Lindgren and L. Walldén, Phys. Rev. Lett. **61**, 2894 (1988).

[10]M. A. Mueller, A. Samsavar, T. Miller, and T.-C. Chiang, Phys. Rev. B **40**, 5845 (1989).

[11]P. O. Gartland and B. J. Slagsvold, Phys. Rev. B **12**, 4047 (1975).

[12]A. P. Shapiro, A. L. Wachs, and T.-C. Chiang, Solid State Chem. **58**, 121 (1986).

[13]J. G. Nelson, S. Kim, W. J. Gignac, R. S. Wiliams J. G. Tobin, S. W. Robey, and D. A. Shirley, Phys. Rev. B **32**, 3465 (1985).

[14]S. Å. Lindgren and L. Walldén, J. Phys. Condens. Matter **1**, 2151 (1989).

[15]P. Heimann and H. Neddermeyer, Solid State Commun. **26**, 279 (1978); C. G. Larsson and J. B. Pendry, J. Phys. C **14**, 3089 (1981).

[16]S. D. Kevan and R. H. Gaylord, Phys. Rev. B **36**, 5809 (1987).

[17]N. V. Smith, Phys. Rev. B **32**, 3549 (1985).

[18]K.-M. Ho, C.-L. Fu, S. H. Liu, D. M. Kolb, and G. Piazza, J. Electroanal. Chem. **150**, 235 (1983).

[19]N. E. Christensen, Phys. Status Solidi B **54**, 551 (1972).

[20]H. Eckardt, L. Fritsche, and J. Noffke, J. Phys. F **14**, 97 (1984).

[21]K. Giesen, F. Hage, F. J. Himpsel, H. J. Riess, and W. Steinmann, Phys. Rev. Lett. **55**, 300 (1985).

[22]D. Schoenberg, Philos. Trans. R. Soc. London, Ser. A **255**, 85 (1962).

[23]D. J. Roaf, Philos. Trans. R. Soc. London, Ser. A **255**, 135 (1962).

[24]M. R. Halse, Philos. Trans. R. Soc. London, Ser. A **265**, 507 (1969).

[25]A. S. Joseph and A. C. Thorsen, Phys. Rev. **138**, A1159 (1965).

[26]See, for example, N. W. Ashcroft and N. D. Mermin, *Solid State Physics* (Saunders College, Philadelphia, 1976), p. 290.

[27]S. D. Kevan, Phys. Rev. Lett. **50**, 526 (1983).